RRP9 suppresses hepatocellular carcinoma progression by inhibiting the PI3K/AKT/mTOR pathway

ZHENGKANG FU[1,2*], MAN LI[2*], KESHUAI DONG[2], JIARUI FENG[1,2] and WEIXING WANG[1,2]

[1]General Surgery Laboratory, Renmin Hospital of Wuhan University, Wuhan, Hubei 430060, P.R. China;
[2]Department of General Surgery, Renmin Hospital of Wuhan University, Wuhan, Hubei 430060, P.R. China

Received August 27, 2025; Accepted March 3, 2026

DOI: 10.3892/ijo.2026.5880

Abstract. Ribosomal RNA processing 9 (RRP9) encodes a WD-repeat domain-containing protein, which is a potential carcinogenic biomarker for various tumors. As a key structural component of small nucleolar ribonucleoproteins, RRP9 serves a key role in ribosome biogenesis by facilitating 18S rRNA processing. Despite its association with the pathogenesis of various malignancies, its function and molecular mechanisms in hepatocellular carcinoma (HCC) remain unknown. The present study aimed to examine the biological role of RRP9 in HCC progression and the underlying regulatory mechanisms. Immunohistochemical and western blot analyses revealed a significant downregulation of RRP9 expression in patients with HCC compared with matched adjacent non-tumorous tissues. To investigate RRP9 biological functions in HCC, stable RRP9-knockdown and -overexpressing isogenic HCC cell line models were established using lentiviral transduction and puromycin selection. Functional assays, including Cell Counting Kit-8 viability, colony formation, wound healing migration and Transwell invasion experiments, consistently demonstrated that RRP9 significantly suppressed HCC cell viability, proliferation, invasion and migration. Transcriptome sequencing and western blot analyses indicated that RRP9 inhibited the PI3K/AKT/mTOR pathway. Furthermore, functional rescue assays using the PI3K activator 740 Y-P and the inhibitor PI3K/AKT/mTOR-IN-2 verified that RRP9 exerts its tumor-suppressive role via this pathway. Protein-protein interaction analysis revealed an association between RRP9 and cyclin A2 (CCNA2). Western blotting confirmed that RRP9 downregulated CCNA2 expression. Additionally, subcutaneous tumorigenesis in mice showed that RRP9 inhibits liver cancer progression via the PI3K/AKT/mTOR signaling pathway.

Correspondence to: Professor Weixing Wang or Professor Jiarui Feng, Department of General Surgery, Renmin Hospital of Wuhan University, 99 Zhangzhidong Road, Wuhan, Hubei 430060, P.R. China
E-mail: sate.llite@163.com
E-mail: rm003008@whu.edu.cn

*Contributed equally

Key words: ribosomal RNA processing 9, hepatocellular carcinoma, PI3K/AKT/mTOR pathway, CCNA2

Introduction

Hepatocellular carcinoma (HCC) is one of the most prevalent types of cancer and represents a notable global public health challenge. It is the sixth most common type of cancer and the third leading cause of cancer-related deaths worldwide, with ~905,000 new cases and 830,000 deaths reported in 2020 (1,2). The progression of liver cancer from a normal liver typically involves three stages: Hepatitis, liver cirrhosis and liver cancer. Key risk factors for these diseases include alcohol consumption, viral infection, aflatoxin exposure and smoking. The treatment options for HCC mainly include surgical resection, chemotherapy, targeted therapy and local embolization (3,4). Despite the availability of these treatments, high recurrence and mortality rates persist. Specifically, the 5-year recurrence rate is >70% following resection, and the overall 5-year survival rate is <20%. These poor outcomes are primarily due to late-stage diagnosis and limited effective treatment options (1). Moreover, recurrence and distant metastasis are notable contributors to treatment failure in advanced liver cancer (5,6). Thus, understanding the molecular mechanisms driving HCC development is key.

Small nucleolar RNAs (snoRNAs) serve a central role in the post-transcriptional modification and maturation of ribosomal RNAs (rRNAs) and other cellular RNAs (7). Rapid cancer cell proliferation requires the production of large quantities of ribosomes to meet the biosynthetic demands (8,9). Elevated ribosome production is not a passive consequence of proliferation, but actively drives cancer progression. Consequently, key regulators of ribosome assembly, such as snoRNAs and their associated proteins, are key players in oncogenesis (10,11). snoRNAs are implicated in various cancers, including breast and colorectal cancer, pancreatic ductal carcinoma and HCC (12-18). Small nuclear RNAs, such as U1-U7, are named for their high uridine content and primarily function in pre-mRNA splicing. By contrast, snoRNAs, including U3 snoRNA, are predominantly localized in the nucleolus and guide the modification and maturation of 18S rRNA (19,20). rRNA processing 9 (RRP9),

also known as U3-55K, is a core subunit of the U3-snoRNP complex (21). Previous studies have demonstrated that RRP9 promotes the development of numerous types of cancer, including pancreatic, colorectal and breast cancer (22-24). The AKT signaling pathway is frequently activated in cancer and RRP9 has been shown to activate the AKT pathway in pancreatic and breast cancer (22,23). RRP9 may promote HCC proliferation through AKT pathway activation (22-24). Given the oncogenic role of RRP9 in other cancers and the key role of dysregulated ribosome biogenesis in HCC, RRP9 may also play a pivotal role in HCC pathogenesis. Thus, the present study aimed to systematically investigate the biological functions of RRP9 in HCC and determine whether its mechanisms align with or differ from those in other types of cancer, thereby identifying potential tissue-specific therapeutic targets.

Materials and methods

Collection and processing of HCC specimens. A total of 216 patients were included in the present study. These patients (176 male and 40 females; age range, 23-77 years) were recruited from Shouyi Campus and East Campus of the Renmin Hospital of Wuhan University (Wuhan, China). To account for potential demographic variations between the two campuses, they were divided into two independent cohorts: Cohort 1 comprised 131 patients (110 males and 21 female; age range, 23-77 years), and cohort 2 comprised 85 patients (66 males and 19 females; age range, 28-75 years). Paired tumorous and matched adjacent non-tumorous tissues (located at least 3 cm away from the tumor margin) were collected from these patients who underwent surgical resection at the Renmin Hospital of Wuhan University (Wuhan, China) from January 2022 to December 2023. The inclusion criteria were as follows: i) Pathologically confirmed primary HCC; and ii) availability of complete clinicopathological and follow-up data. The exclusion criteria were: i) Patients who had received preoperative anti-cancer treatments (such as chemotherapy, radiotherapy, targeted therapy, or local embolization); and ii) presence of other primary malignancies. The present study was conducted in accordance with the principles of the Declaration of Helsinki and was approved by the Ethics Committee of Renmin Hospital of Wuhan University (Wuhan, China; approval no. WDRY2022-K013). Written informed consent was obtained from all patients prior to surgery and sample collection.

Cell culture and transfection. Huh7 (cat. no. CL-0120) and Hep-3B (cat. no. CL-0102) cell lines were purchased from Wuhan Pricella Biotechnology Co. MHCC 97h (cat. no. CBP60227) and HLF (cat. no. CBP60589) cell lines were purchased from Nanjing Kebai Biotechnology Co., Ltd. Snu449 (cat. no. CC0105) cells were purchased from Saiku Biotechnology Co. 97h is a highly metastatic cell line derived from a patient with HCC lung metastasis. Huh7 is a well-differentiated, non-metastatic cell line with mutant p53. Hep-3B is a poorly differentiated cell line deficient in p53 expression and harboring an integrated hepatitis B virus genome. HLF is a highly metastatic cell line with mutant p53, while Snu449 is derived from a primary tumor and also carries a mutant p53. 97h, Huh7, Hep-3B and HLF cells were cultured in DMEM supplemented with 10% FBS, while Snu449 cells were maintained in RPMI-1640 medium (all Gibco; Thermo Fisher Scientific, Inc.) with 10% FBS. All cell lines were incubated under standard conditions (37˚C, 5% CO_2).

For lentiviral production, 293T cells (Wuhan Pricella Biotechnology; cat. no. CL-0001) were co-transfected with 10 μg 2nd-generation RRP9, CCNA2 or their respective negative control lentiviral plasmids and helper plasmids (psPAX2 and pMD2.G; ratio 4:3:1; MiaoLing Plasmid) using Lipo8000™ (Beyotime Biotechnology; cat. no. C0533) at 37˚C for 10 h. Viral particles collected at 48 h were used to infect HCC cells at an MOI of 10 for 24 h at 37˚C with 5% CO_2. Stable transductants were selected with 10 μg/ml puromycin, maintained at 2 μg/ml and used for subsequent experiments 7 days post-transduction.

740 Y-P is a cell-permeable peptide that mimics a tyrosine-phosphorylated segment of the platelet-derived growth factor receptor, thereby directly activating PI3K by binding its SH2 domains (34,35). Cells were treated with 20 μM 740 Y-P or 10 μM PI3K/AKT/mTOR-IN-2 for 24 h at 37˚C (25,26).

Immunohistochemistry. Tissue specimens, fixed in 4% paraformaldehyde at room temperature for 24 h, were embedded in paraffin and cut into 1.5 μm thick sections. The sections were deparaffinized in xylene and rehydrated through a descending alcohol series. Antigen retrieval was performed by heating in Tris-EDTA antigen repair solution (pH 9.0) at 95˚C for 15 min. Endogenous peroxidase activity was quenched with 3% hydrogen peroxide for 15 min, followed by membrane permeabilization using 0.2% Triton X-100 for 45 min. Non-specific binding was blocked with 10% donkey serum (Beijing Solarbio Biotechnology; cat. no. SL050) at room temperature for 1 h. Subsequently, sections were incubated at 4˚C for 12-16 h with primary antibodies, including anti-RRP9 (Santa Cruz Biotechnology; 1:50; cat. no. sc-100592) or Ki-67 (Wuhan Pricella Biotechnology; 1:50; cat No. 27309-1-AP). Sections were incubated with an HRP-conjugated secondary antibody (Thermo Fisher Scientific Inc.; 1:500; cat. no. 31460) using the MaxVision detection reagent at room temperature for 30 min. Immunoreactivity was visualized using a DAB Chromogen detection kit (Abcam). Nuclei were counterstained with hematoxylin at room temperature for 5 min. Slides were examined and imaged using a light microscope (Olympus Corporation), with quantitative analysis performed using ImageJ software (version 1.8.0; National Institutes of Health).

Tissue microarray. To evaluate RRP9 expression in the clinical cohorts, a tissue microarray was constructed using the collected formalin-fixed, paraffin-embedded (FFPE) HCC and matched adjacent non-tumor tissues. Due to the large sample size exceeding the maximum capacity of a single recipient block, the cohort samples were distributed across three independent TMA blocks to preserve tissue integrity and ensure high-quality sectioning. To minimize technical variations and ensure direct comparability of the data, all three TMA blocks were prepared, sectioned, and immunohistochemically stained simultaneously using an identical protocol.

TUNEL assay. To evaluate apoptosis in the xenograft tumor tissues, TUNEL) assay was performed using a TUNEL Apoptosis Assay Kit (Beyotime Biotechnology; cat. no. C1086) according to the manufacturer's instructions.

Western blotting. Total protein was extracted from cultured cells and HCC tissues using RIPA lysis buffer (Beyotime Biotechnology) supplemented with phosphatase and protease inhibitors (including PMSF). Protein concentrations were determined using a BCA protein assay kit (Thermo Fisher Scientific). Equal amounts of protein (20 μg per lane) were separated via 10% SDS-PAGE. Proteins were then electrotransferred onto PVDF membranes. The membranes were blocked with 5% non-fat milk for 1 h at room temperature, and incubated overnight at 4˚C with primary antibodies against the target proteins and the internal reference, RRP9 (Santa Cruz Biotechnology; 1:50; cat. no. sc-100592); E-cadherin (Proteintech Group, Inc.; 1:5,000, cat. no. 22018-1-AP), N-cadherin (Proteintech Group, Inc.; 1:5,000, cat. no. 20874-1-AP), Vimentin (Proteintech Group, Inc.; 1:5,000, cat. no. 10366-1-AP), Snail-1 (Proteintech Group, Inc.; 1:5,000, cat. no. 13099-1-AP), Bax (Proteintech Group, Inc.; 1:5,000, cat. no. 50599-2-Ig), Bcl-2 (Proteintech Group, Inc.; 1:5,000, cat. no. 12789-1-AP), PI3K (Proteintech Group, Inc.; 1:5,000, cat. no. 20584-1-AP), AKT (Proteintech Group, Inc.; 1:5,000, cat. no. 10176-2-AP), mTOR (1:5,000, cat. no. 20657-1-AP) and GAPDH (1:5,000; cat. no. 60004-1-Ig; all Proteintech Group, Inc). Following three washes with TBST containing 0.1% Tween-20, the membranes were incubated with HRP-conjugated secondary antibody (1:5,000; Proteintech Group, Inc.), HRP-Goat Anti-Mouse Secondary Antibody (Proteintech Group, Inc.; 1:5,000, cat. no. RGAR001) and HRP-Goat Anti-Rabbit Secondary Antibody (Proteintech Group, Inc.; 1:5,000, cat. no. RGAM001) for 1 h at room temperature. Protein bands were visualized using an enhanced chemiluminescence kit (Proteintech Group, Inc.). Densitometric analysis was performed using ImageJ software (version 1.8.0).

Co-immunoprecipitation. Cells were lysed in cold IP buffer (Beyotime Biotechnology; cat. no. P0013) containing protease inhibitors. Total cell lysates were incubated with primary antibodies against RRP9, CCNA2, or normal IgG (as a negative control) at 4˚C overnight. Protein A/G magnetic (Beyotime Biotechnology; cat. no. P2108; 25 μl) beads were added to capture the immune complexes. After washing three times with lysis buffer, the precipitated proteins were eluted by boiling in SDS loading buffer and analyzed by western blotting.

Cell Counting Kit (CCK)-8 assay. After establishing stable RRP9-overexpression and RRP9-knockdown models, the cells were seeded into 96-well culture plates at an initial density of $8x10^3$ cells/well in quadruplicate. The cells were cultured in DMEM supplemented with 10% FBS and incubated under standard conditions (37˚C, 5% CO_2). CCK-8 solution (Biosharp Life Sciences) was added at 0, 24, 48 and 72 h according to the manufacturer's protocol. Following 120 min incubation, optical density was measured at 450 nm using a multi-mode microplate reader.

Colony formation assay. Stable RRP9-overexpressing and -knockdown and control HCC cells were plated in 6-well culture dishes at a density of 1,000 cells/well and maintained for 14 days under standard conditions. Cells were fixed with 4% paraformaldehyde for 15 min at room temperature. The colonies were stained with 2% crystal violet for 20 min at room temperature, followed by rinsing with distilled water. Images were captured using a digital imaging system. The number of colonies (clusters of >50 cells) was quantified using ImageJ software (version 1.8.0).

Transwell assay. To evaluate cell migration and invasion, Transwell chambers with 8.0 μm porous membranes (Corning, Inc.) were used. For the migration assay, $4x10^5$ cells in serum-free medium [DMEM (Thermo Fisher Scientific Inc.; cat. no. 11965092) for HLF, 97h, and Huh7 cells; RPMI-1640 (Thermo Fisher Scientific Inc.; cat. no. 11875119) for Snu449 cells] was added to the upper chamber, while the lower chamber was filled with culture medium supplemented with 10% FBS. In the invasion assay, the upper chamber was pre-coated with Matrigel at 37˚C for 2 h prior to seeding $5x10^5$ cells in the aforementioned serum-free media; the lower chamber contained medium with 10% FBS as a chemoattractant. After 24-48 h incubation at 37˚C, cells that had migrated through the membrane were fixed with 4% paraformaldehyde at room temperature for 20 min. The cells were stained with 0.1% crystal violet solution at room temperature for 20 min and quantified using a light microscope.

Wound healing assay. Migration of Snu449, HLF, 97h and Huh7 cells was evaluated using a wound healing assay. A uniform scratch was made in a cell monolayer at >90% confluence using a sterile pipette tip. Following three washes with PBS, the cells were maintained in serum-free medium [HLF, 97h and Huh7 cell cultivated in DMEM, Snu449 cultivated in RPMI-1640 (Thermo Fisher Scientific Inc.; cat. no. 11875119)] for 48 h at 37˚C. Images were captured at 0 and 48 h using a light microscope (Olympus). The relative wound closure rate was determined by measuring the wound width at both time points and calculating the percentage reduction using Adobe Photoshop software (version 26.8.0; Adobe Systems, Inc.).

RNA sequencing. Total RNA was extracted from HLF cells of the wild-type (WT) and RRP9-overexpressing (RRP9-OE) groups using TRIzol. Three independent biological replicates were performed for each group to ensure statistical reliability. RNA quality and quantity were assessed using a Fragment Analyzer, Agilent 2100 Bioanalyzer (Agilent Technologies, Inc.), or Qseq-400 (BiOptic, Inc.). The DESeq2 software package (v1.34.0) was employed to identify differentially expressed genes (DEGs) for subsequent investigations. Detailed RNA sequencing procedures, including extraction, library preparation, quality control, and data analysis, are provided in Supplementary Material 1. Venn diagrams were generated using the VennDiagram R package (version_1.8; github.com/) and Gene Ontology (GO; geneontology.org/) and Kyoto Encyclopedia of Genes and Genomes (KEGG; kegg.jp/) enrichment analyses were performed using the clusterProfiler R package (version 4.18.4; https://github.com/).

Protein-protein interaction (PPI) network construction. Differentially expressed genes (DEGs) [adjusted P-value <0.05 and |log2(fold-change)|>1] identified by RNA sequencing were imported into the STRING database (cn.string-db.org/) with a minimum interaction score of 0.9. The data were processed in Cytoscape 3.10.3 (cytoscape.org/), and core targets of the PPI network were identified by calculating the degree values.

Xenograft tumor model in nude mice. Female immunocompromised BALB/c nude mice (age, 4 weeks; weight, 16-18 g) were obtained from Bainter Biotechnology (Wuhan, China). The mice were housed under specific pathogen-free conditions at 22±2˚C and 50±10% humidity, with a 12-h light/dark cycle and *ad libitum* access to food and water. The animals (n=18) were randomly divided into three experimental groups (n=6): WT, OE and OE + 740 Y-P. Tumor xenografts were generated by subcutaneously implanting $5x10^6$ HLF cells suspended in 100 μl PBS into the right flank region. Tumor growth was monitored weekly, with specimens collected after 4 weeks. Tumor dimensions were recorded and volumes were calculated using the standard ellipsoid formula: $V=(L \times W^2)/2$, where L is the longest diameter and W is the perpendicular width. The humane endpoints included a maximum tumor volume of 1,500 mm^3, severe tumor ulceration or >20% loss of initial body weight. During the 4-week experimental period, none of the mice reached these humane endpoints, and no animals were prematurely euthanized. All procedures involving laboratory animals were conducted in accordance with protocols approved by the Animal Research Ethics Committee of Wuhan University People's Hospital (Wuhan, China; approval no. WDRM20250303).

Statistical analysis. The experimental data were processed and visualized using SPSS software (version 22.0; IBM Corp.) and GraphPad Prism (version 9.0; Dotmatics). Comparisons between two groups were performed using paired or unpaired t-test. For comparisons involving >2 groups, a one-way ANOVA followed by Tukey's honestly significant difference post hoc test was used. χ^2 test was used to analyze the association between target gene expression and clinicopathological characteristics. Overall survival curves were plotted using the Kaplan-Meier method, and the differences between the survival curves were evaluated using the log-rank test. All data are presented as the mean ± standard deviation of ≥3 independent experiments. P<0.05 was considered to indicate a statistically significant difference.

Results

alidation of RRP9 expression in clinical samples. The expression of RRP9 in the samples was assessed using western blotting, revealing lower RRP9 expression in cancer compared with adjacent non-tumor tissues (Fig. 1A). Tissue microarray analysis of both cohorts showed reduced RRP9 expression in HCC tissues compared with adjacent non-tumor tissue (Figs. 1B and S1), consistent with western blot results. Based on RRP9 expression in HCC tissue, the patients were categorized into high- and low-expression groups using the median score of 133 as the cut-off value. The demographic and clinicopathological characteristics of these groups are summarized in Table I. Lower RRP9 expression in HCC was associated with more tumor nodules, Barcelona Clinic Liver Cancer stage, tumor size and Tumor-Node-Metastasis stage (27,28) (Table I). Kaplan-Meier survival analysis revealed that patients with higher RRP9 expression had significantly longer overall survival (Fig. 1C).

RRP9 inhibits HCC cell proliferation, migration and invasion. Western blot analysis was performed to assess RRP9 expression in HCC cell lines. RRP9 levels were lower in HLF and Snu449 cells, while higher levels were observed in Huh7 and 97h cells (Fig. 2E). RRP9 was overexpressed in cell lines with low basal expression (HLF and Snu449) to evaluate its tumor-suppressive potential, and knocked down in high-expressing lines (Huh7 and 97H) to assess its tumor-promoting effects. Western blotting confirmed the successful construction of these cell lines (Figs. 2F and G, S3A-D). The CCK-8 assay demonstrated RRP9-OE reduced short-term proliferative activity in Snu449 and HLF cells (Fig. 2A and B), while RRP9 knockdown increased short-term proliferative activity in Huh7 and 97h cells (Fig. 2C and D). RRP9-OE inhibited colony formation (Fig. 2H and I), while RRP9 knockdown promoted colony formation (Fig. 2J and K). These results suggested that RRP9 can inhibit short-term and long-term proliferation of HCC cells.

The effect of RRP9 on the migration and invasion of HCC cells was evaluated using wound healing and Transwell assay. Wound healing assays showed that RRP9-OE inhibited migration in Snu449 and HLF cells, while RRP9 knockdown enhanced migration in Huh7 and 97h cells (Fig. 3A-D). Transwell assay confirmed RRP9-OE inhibited migration and invasion in Snu449 and HLF cells, whereas RRP9 knockdown decreased migration and invasion in Huh7 and 97h cells (Fig. 3E-H).

RRP9 promotes apoptosis and inhibits epithelial-mesenchymal transition (EMT) in HCC. EMT marker expression was analyzed by western blotting, revealing that RRP9-OE decreased the levels of Snail-1, N-cadherin and vimentin in Snu449 and HLF cell lines, while increasing E-cadherin expression (Fig. 4A). By contrast, RRP9 knockdown in Huh7 and 97H cells significantly increased the expression of Snail-1, N-cadherin, and vimentin, while decreasing E-cadherin levels (Fig. 4B). To investigate the impact of RRP9 on apoptosis, the expression of Bax and Bcl-2 was measured. The results demonstrated a decrease in the expression of anti-apoptotic factor Bcl-2 and an increase in the pro-apoptotic factor Bax in Snu449 and HLF cells following RRP9 OE (Fig. 4C). Conversely, RRP9 knockdown in Huh7 and 97H cells significantly increased the expression of the anti-apoptotic factor Bcl-2 and decreased the expression of the pro-apoptotic factor Bax (Fig. 4D). These results suggested that RRP9 suppressed HCC cell invasion and migration, promoted apoptosis and inhibited EMT.

RRP9 regulates HCC progression via the PI3K/AKT/mTOR signaling pathway. To elucidate the mechanism underlying the action of RRP9 action in HCC, transcriptome sequencing was performed on WT and RRP9-OE HLF cells. The sequencing results revealed a number of DEGs following RRP9 OE (Fig. 5A). The Venn diagram indicated that 15,926 genes

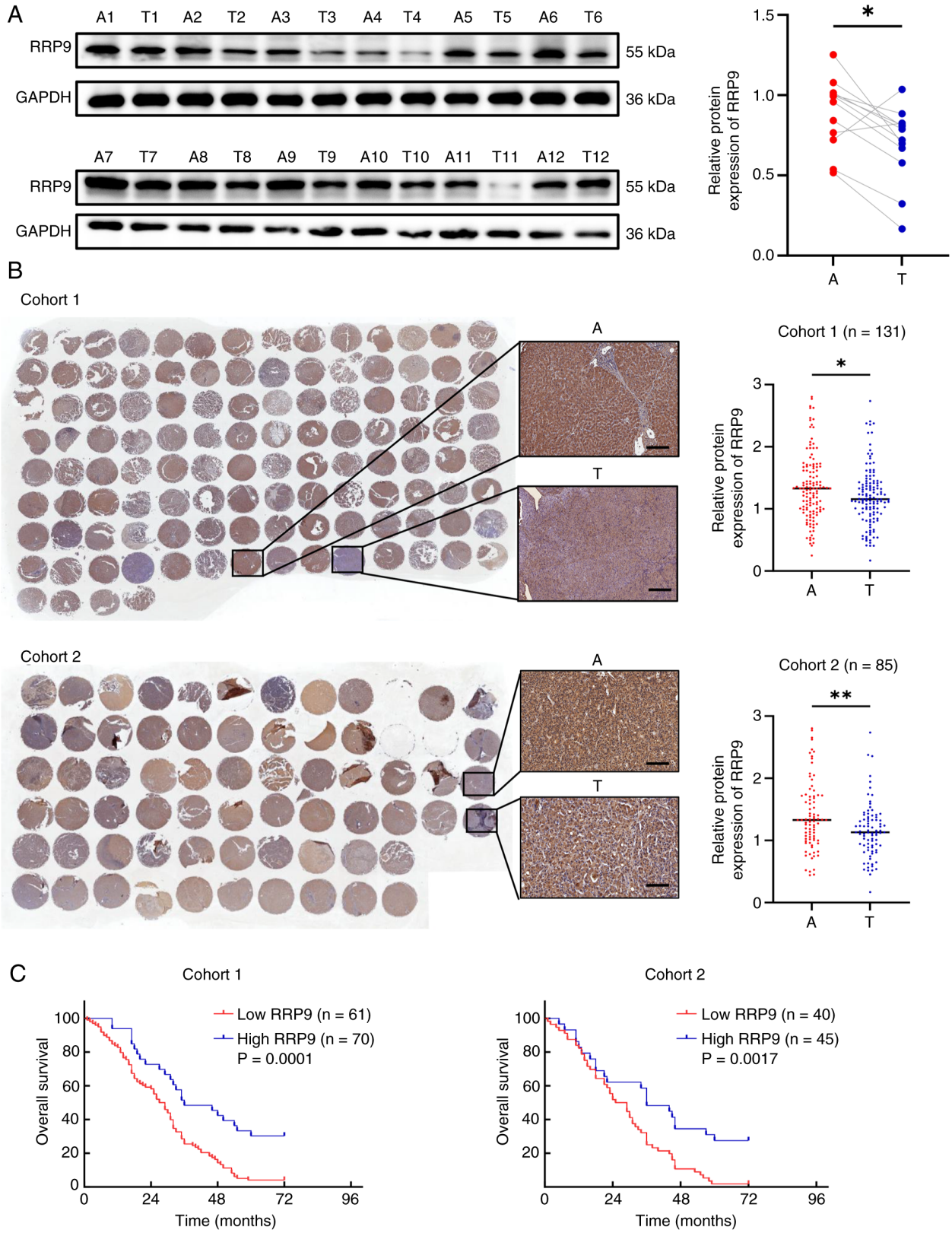

Figure 1. RRP9 expression in hepatocellular carcinoma tissue. (A) Western blot analysis of RRP9 protein levels in patients with liver cancer. (B) Representative immunohistochemical staining of RRP9 expression in cohort 1 and 2 liver cancer tissue microarrays. (C) Kaplan-Meier survival curve showing overall survival (log-rank test). Scale bar, 100 μm. *P<0.05, **P<0.01. RRP9, ribosomal RNA processing 9; A, adjacent; T, tumor.

were shared between the WT and OE groups (Fig. 5B). Gene Ontology enrichment analysis highlighted significant enrichment of DEGs in processes associated with the cell cycle, 'sites of DNA damage' and 'extracellular exosome' (Fig. 5C). Kyoto Encyclopedia of Genes and Genomes enrichment analysis showed that RRP9-OE influenced pathways such as 'PI3K-Akt signaling', 'pathways in cancer', 'AMPK signaling pathway', 'mTOR signaling pathway', 'MAPK signaling pathway' and

Table I. Clinicopathological characteristics of patients with low- and high-RRP9 expression in primary liver cancer tissue.

	Cohort 1 (n=131)		Cohort 2 (n=85)		P-value	
Characteristic	Low	High	Low	High	Group 1	Group 2
Cases	61	70	40	45		
Age, years					0.7982	0.5352
≤60	45	53	25	31		
>60	16	17	15	14		
Sex					0.2889	0.9755
Male	49	61	31	35		
Female	12	9	9	10		
Diagnosis					0.8398	0.3429
HCC	58	66	40	44		
ICC	3	4	0	1		
Child-Pugh score					0.0333	0.0001
A	49	65	11	31		
B	12	5	29	14		
BCLC stage					0.0092	0.0010
A	33	55	9	25		
B	8	6	14	15		
C	20	9	17	5		
Number of tumors					0.0013	0.0131
≤3	22	45	12	33		
>3	39	25	28	12		
Tumor diameter, cm					0.0139	0.0005
≤5	13	29	9	27		
>5	48	41	31	18		
TNM stage					0.0144	0.0089
I	31	54	10	18		
II	1	1	5	15		
III	25	14	15	7		
IV	4	1	10	5		

P-values are from χ^2 test. BCLC, RRP9, ribosomal RNA processing 9; ICC, intrahepatic cholangiocarcinoma; HCC, Hepatocellular Carcinoma.

'Ras signaling pathway' (Fig. 5D). To identify core regulatory nodes within the RRP9-mediated transcriptomic changes, 465 DEGs were selected for PPI network analysis. These DEGs were imported into the STRING database and a core target network containing 25 targets and 96 edges was constructed using Cytoscape 3.10.3. Cyclin A2 (CCNA2; degree=10) was associated with RRP9 (Fig. 5E). Given that CCNA2 is a well-established key regulator of the cell cycle and its dysregulation is frequently implicated in cancer progression (29-31), it was selected for experimental validation to explore its functional connection to RRP9 in HCC.

Given the key role of the PI3K/AKT/mTOR signaling pathway in cancer, the expression of PI3K, AKT, mTOR, phosphorylated (p-)PI3K, p-AKT and p-mTOR was assessed by western blotting. The ratios of p-PI3K/PI3K, p-AKT/AKT and p-mTOR/mTOR were decreased in RRP9-OE Snu449 and HLF cell lines, suggesting inhibition of the PI3K/AKT/mTOR pathway (Fig. 6A). Conversely, RRP9 knockdown in Huh7 and 97H cells significantly increased the ratios of p-PI3K/PI3K, p-AKT/AKT and p-mTOR/mTOR (Fig. 6B). To investigate the association between RRP9 and CCNA2, proteins were extracted from RRP9-OE, RRP9-knockdown, and wild-type cells. Western blot analysis revealed that RRP9-OE decreased CCNA2 protein levels (Fig. 6C), whereas RRP9 knockdown led to increased CCNA2 expression (Fig. 6D). Co-immunoprecipitation (Co-IP) experiments confirmed that RRP9 interacted with CCNA2 in both 293T and 97h cell lines (Fig. S2). Following the validation of CCNA2 knockdown and overexpression via western blotting (Fig. S3E and F), we observed that CCNA2 overexpression increased the ratios of p-PI3K/PI3K, p-AKT/AKT, and p-mTOR/mTOR, whereas CCNA2 knockdown exerted the opposite inhibitory effect, demonstrating that CCNA2 positively regulates the PI3K/AKT/mTOR signaling pathway (Fig. S2D and E).

It was hypothesized that RRP9 regulates EMT in HCC cells via the PI3K/AKT/mTOR pathway. Therefore, Snu449

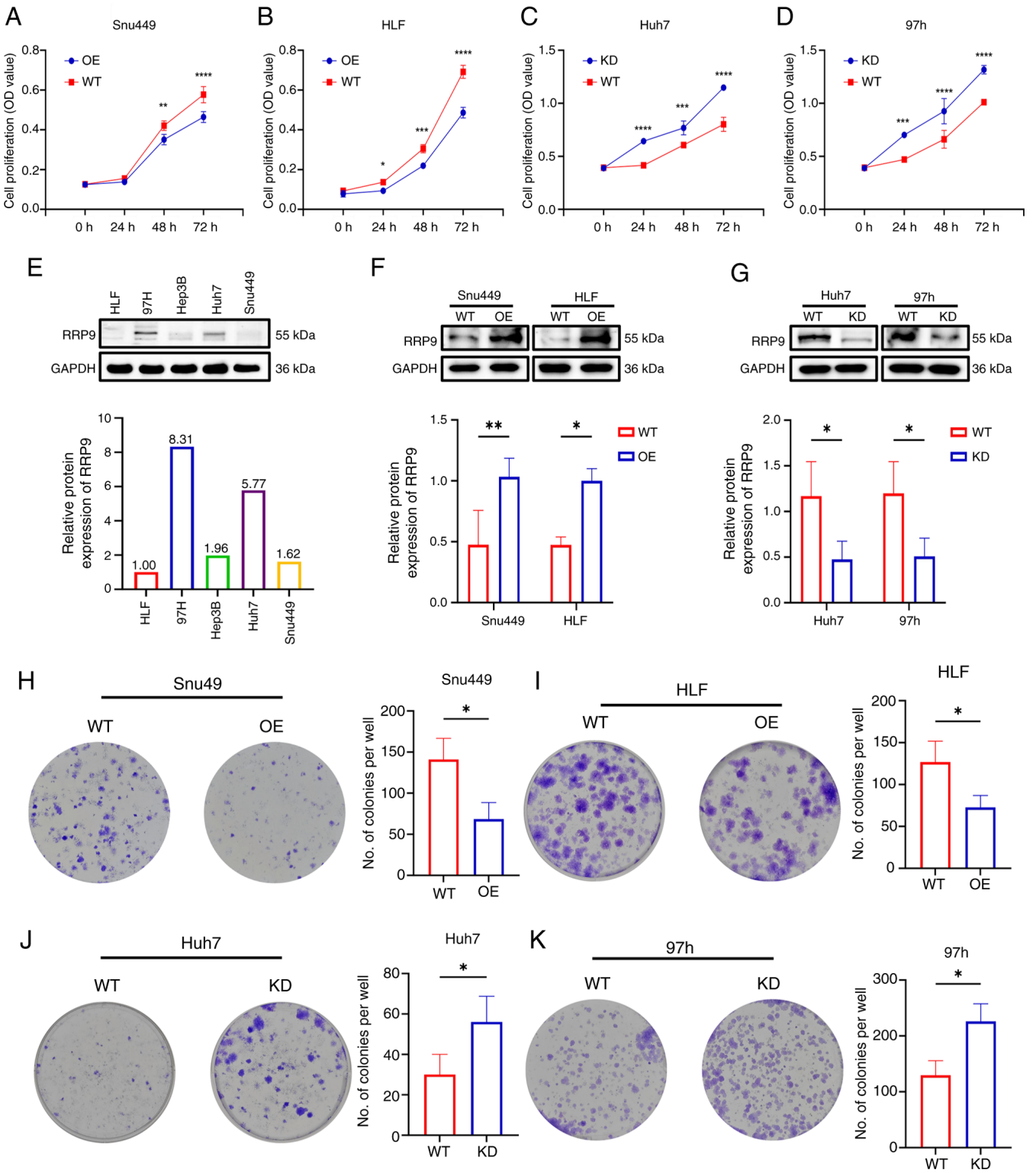

Figure 2. Impact of RRP9 on HCC proliferation. (A) CCK-8 assay assessing Snu449 and (B) HLF cell proliferation following RRP9 overexpression. (C) CCK-8 assay assessing Huh7 cell proliferation following RRP9 knockdown. (D) CCK-8 assay assessing 97h cell proliferation following RRP9 knockdown. (E) Western blot analysis of basal RRP9 expression in liver cancer cell lines. (F) Western blot validation of RRP9 overexpression efficiency. (G) Western blot validation of RRP9 knockdown efficiency. (H) Colony formation assay evaluating Snu449 and (I) HLF cell proliferation following RRP9 overexpression and (J) Huh7 cell proliferation following RRP9 knockdown. (K) Colony formation assay evaluating 97h cell proliferation following RRP9 knockdown. *P<0.05, **P<0.01, ***P<0.001, ****P<0.0001 vs. WT group. RRP9, ribosomal RNA processing 9; HCC, hepatocellular carcinoma; WT, wild-type; OE, overexpression; KD, knockdown; OD, optical density.

and HLF cells were treated with the PI3K activator 740 Y-P and Huh7 and 97h cells with the PI3K/AKT/mTOR pathway inhibitor PI3K/AKT/mTOR-IN-2. Western blotting showed that 740 Y-P activated the PI3K/AKT/mTOR pathway and the inhibitory effect of RRP9-OE on EMT was reversed following treatment with 740 Y-P (Fig. 7A). To confirm that RRP9

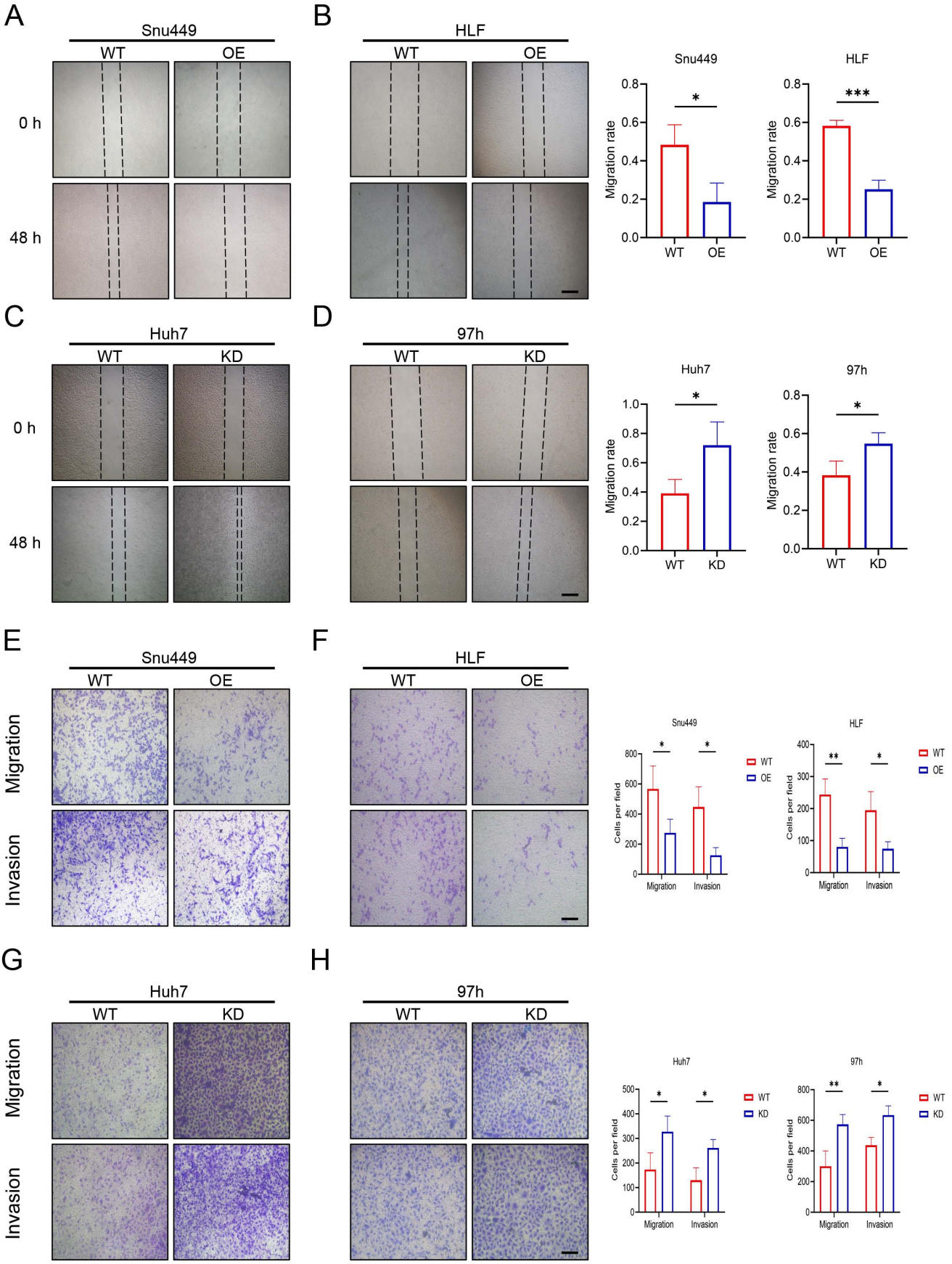

Figure 3. Impact of RRP9 on hepatocellular carcinoma cell migration and invasion. (A) Wound healing assay evaluating migration in Snu449 and (B) HLF cells following RRP9 overexpression. (C) Wound healing assay evaluating migration in Huh7 cells following RRP9 knockdown. (D) Wound healing assay evaluating migration in 97h cells following RRP9 knockdown. (E) Transwell assays assessing migration and invasion of Snu449 cells following RRP9 overexpression. (F) Transwell assays assessing migration and invasion of HLF cells following RRP9 overexpression. (G) Transwell assays assessing migration and invasion of Huh7 and (H) Transwell assays assessing migration and invasion of 97h cells following RRP9 knockdown. Scale bar, 100 μm. *P<0.05, **P<0.01, ***P<0.001. RRP9, ribosomal RNA processing 9; WT, wild-type; KD, knockdown; OE, overexpression.

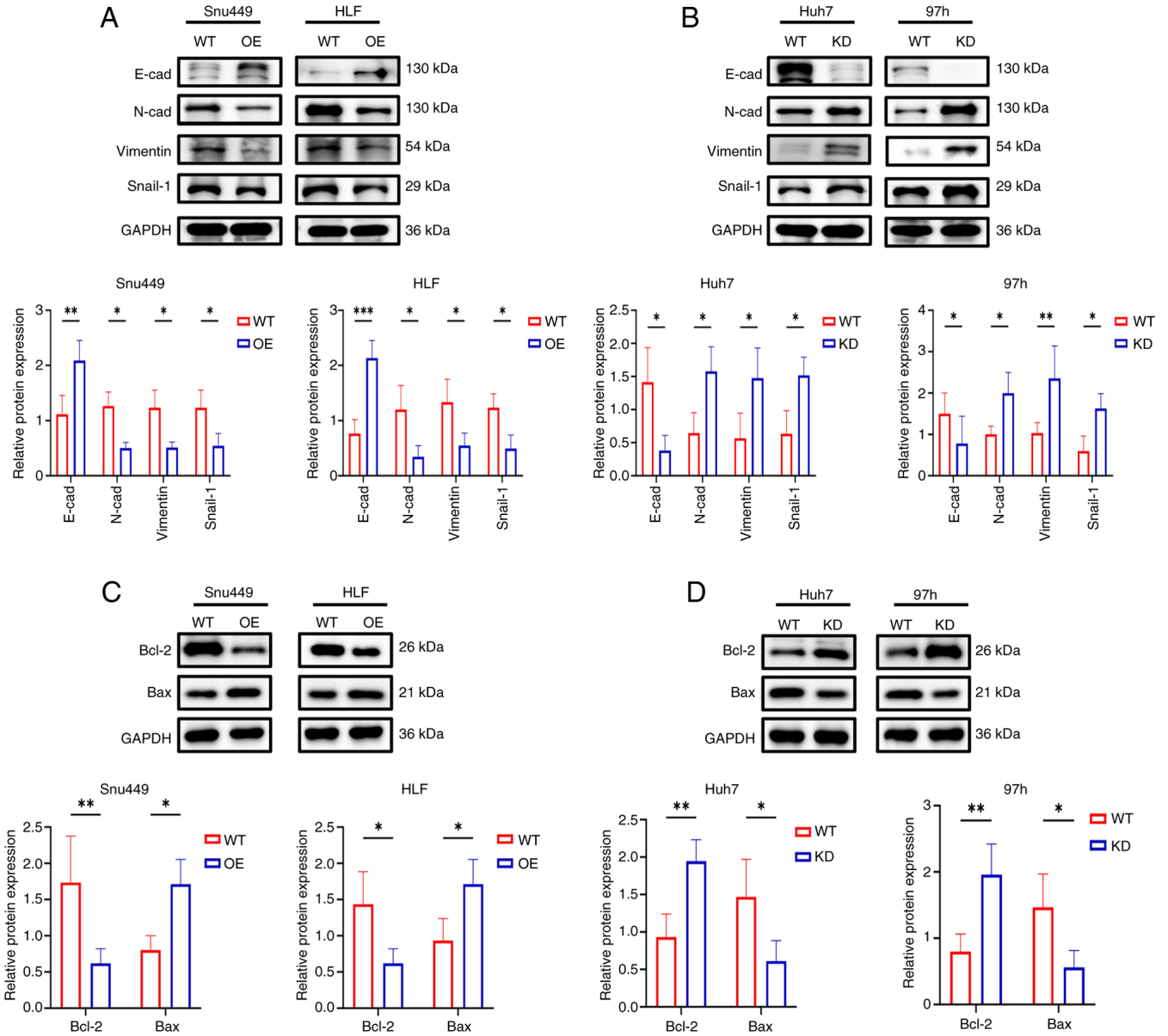

Figure 4. Effect of RRP9 on apoptosis- and EMT-associated protein in HCC. (A) Western blot analysis of EMT-associated proteins (E-cad, N-cad, vimentin, and Snail-1) in Snu449 and HLF cells following RRP9 overexpression and (B) Western blot analysis of EMT-associated proteins (E-cad, N-cad, vimentin, and Snail-1) in Huh7 and 97h cells following RRP9 knockdown and (C) apoptosis-related proteins (Bax and Bcl-2) in Snu449 and HLF cells following RRP9 overexpression and (D) Western blot analysis of apoptosis-related proteins (Bax and Bcl-2) in Huh7 and 97h cells following RRP9 knockdown. *P<0.05, **P<0.01. EMT, epithelial-mesenchymal transition; HCC, hepatocellular carcinoma; cad, cadherin; WT, wild-type; OE, overexpression.

knockdown regulated EMT via the PI3K/AKT/mTOR pathway, Huh7 and 97h cells were treated with PI3K/AKT/mTOR-IN-2. Western blotting demonstrated that PI3K/AKT/mTOR-IN-2 inhibited the promotion of EMT induced by RRP9 KD (Fig. 7B). These results suggested that RRP9 regulates EMT in HCC cells through the PI3K-AKT/mTOR signaling pathway.

It was hypothesized that RRP9 affected the migration and invasion of HCC cells via the PI3K/AKT/mTOR signaling pathway. Snu449 and HLF cells overexpressing RRP9 were treated with 740 Y-P. The wound healing and Transwell assays revealed that 740 Y-P reversed the inhibitory effect of RRP9-OE on the migration and invasion of HCC cells (Fig. 8A-D).

Huh7 and 97h cells with RRP9 knockdown were treated with PI3K/AKT/mTOR-IN-2; wound healing and Transwell assays indicated that PI3K/AKT/mTOR-IN-2 inhibited the enhanced migratory and invasive capacity induced by RRP9 knockdown (Fig. 9A-D). In summary, RRP9 regulated HCC cell migration, invasion and EMT by regulating the PI3K/AKT/mTOR signaling pathway.

RRP9 suppresses tumor growth in vivo by inhibiting the PI3K/AKT/mTOR signaling pathway. To investigate the role of RRP9 in tumor progression, an *in vivo* model was constructed. Nude mice were divided into three groups: WT, OE and OE + 740 Y-P. HLF cells, which exhibited one of the lowest basal levels of RRP9 protein, were selected for xenograft experiments to maximize the phenotypic difference between the OE and WT groups. RRP9-OE significantly inhibited tumor growth in a subcutaneous xenograft model, with marked

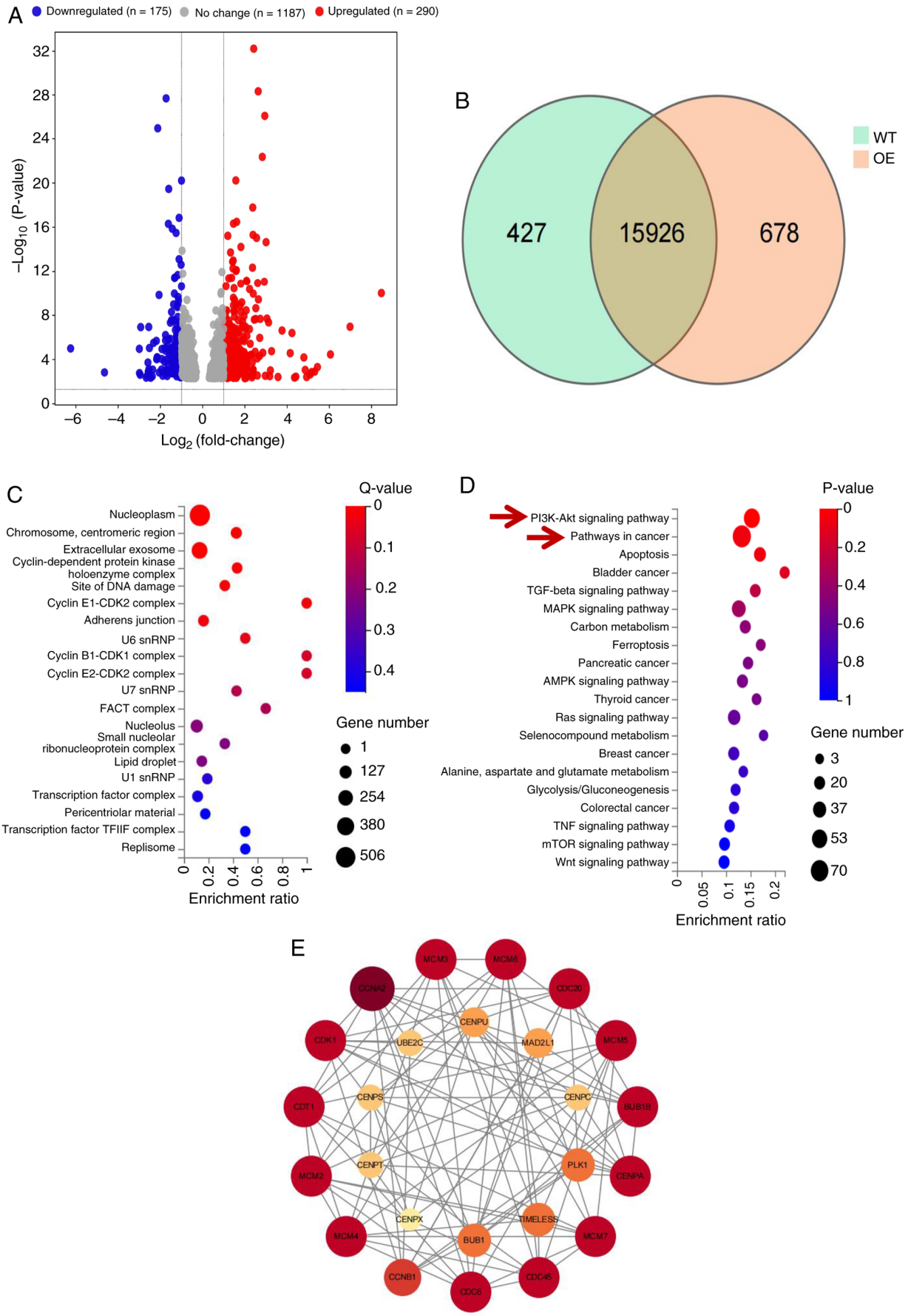

Figure 5. RNA sequencing identified the cell cycle and PI3K/AKT/mTOR signaling pathways as potential mechanisms by which ribosomal RNA processing 9 regulates hepatocellular carcinoma. (A) Volcano plot illustrating differentially expressed genes from transcriptomic sequencing. (B) Venn diagram depicting the intersecting genes. (C) Gene Ontology and (D) Kyoto Encyclopedia of Genes and Genomes enrichment analysis. (E) Protein-protein interaction network diagram. The color represents the connectivity degree of the proteins, ranging from 10 to 4. WT, wild-type; OE, overexpression

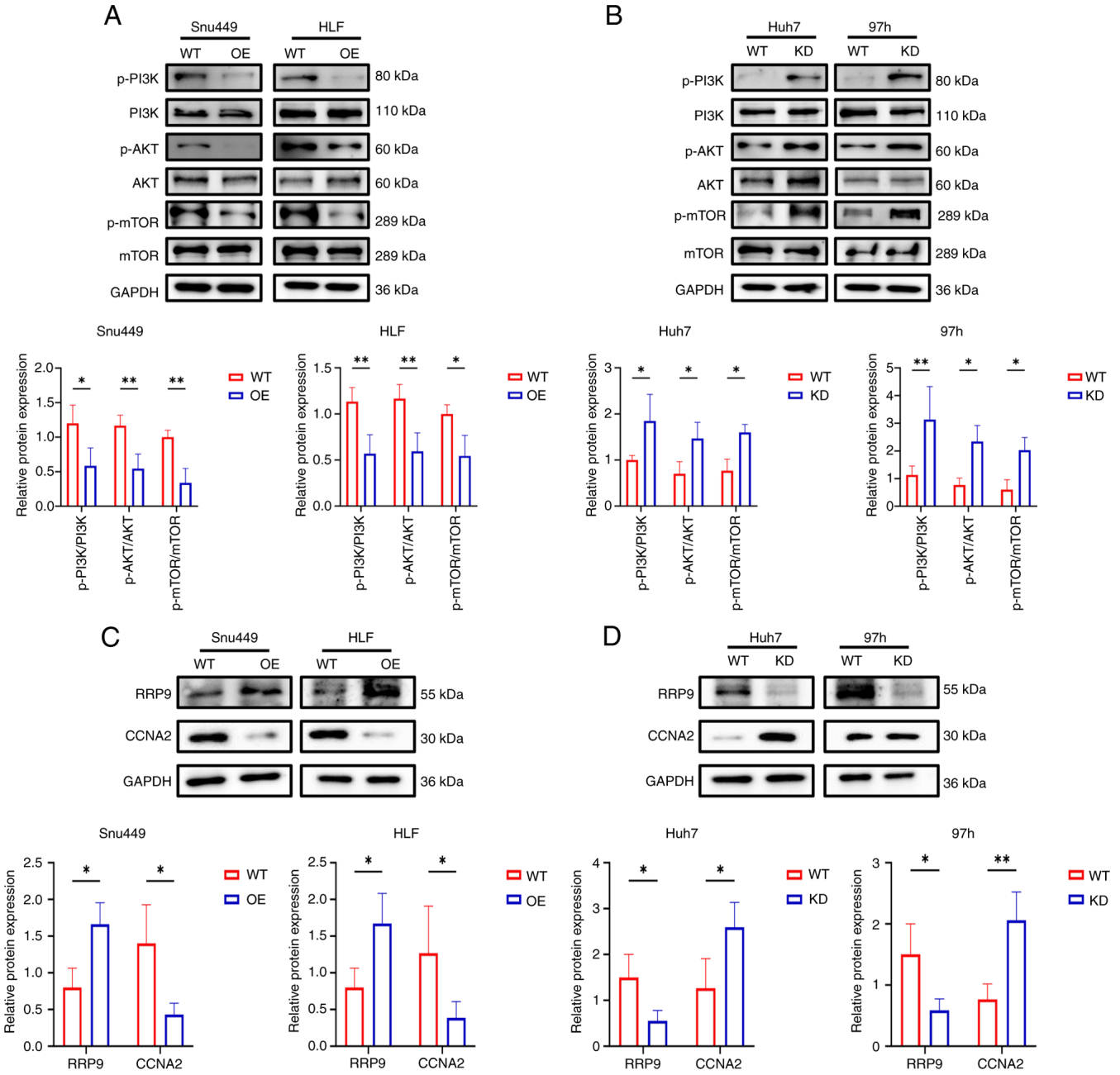

Figure 6. RRP9 regulates the PI3K/AKT/mTOR signaling pathway and CCNA2. (A) Western blot analysis of PI3K/AKT/mTOR signaling pathway proteins in Snu449 and HLF cells following RRP9 overexpression and (B) Huh7 and 97h cells following RRP9 knockdown. (C) Western blot analysis of CCNA2 protein expression in Snu449 and HLF cells following RRP9 overexpression and (D) Western blot analysis of CCNA2 protein expression in Huh7 and 97h cells following RRP9 knockdown. *P<0.05, **P<0.01. RRP9, ribosomal RNA processing 9; CCNA2, cyclin A2; WT, wild-Type; OE, overexpression; p-, phosphorylated-; KD, knockdown.

decreases in both tumor weight and volume. However, 740 Y-P reversed the inhibitory effect of RRP9-OE on tumor growth (Fig. 10A-C, E), suggesting that RRP9 suppressed tumor growth *in vivo* via the PI3K/AKT/mTOR signaling pathway. TUNEL staining showed that RRP9 promoted apoptosis in subcutaneous tumors (Fig. 10D). Western blot analysis confirmed effective OE of RRP9 in xenograft tumors, with increased E-cadherin and decreased N-cadherin expression in the OE group compared with the WT group (Fig. 10F). Immunohistochemical analysis revealed that the OE group exhibited decreased expression of the proliferation marker Ki-67 and the mesenchymal marker N-cadherin, alongside increased expression of the epithelial marker E-cadherin, compared with the WT group (Fig. 10G). These results indicated that RRP9 effectively suppressed tumor growth *in vivo*.

Discussion

Liver cancer, one of the most common and deadly types of malignancy, is characterized by aggressive biology, rapid progression and a tendency for early metastasis. Conventional therapies provide limited benefits, highlighting the need for new molecular targets and effective treatments (32,33). EMT is a cell reprogramming process in which epithelial cells

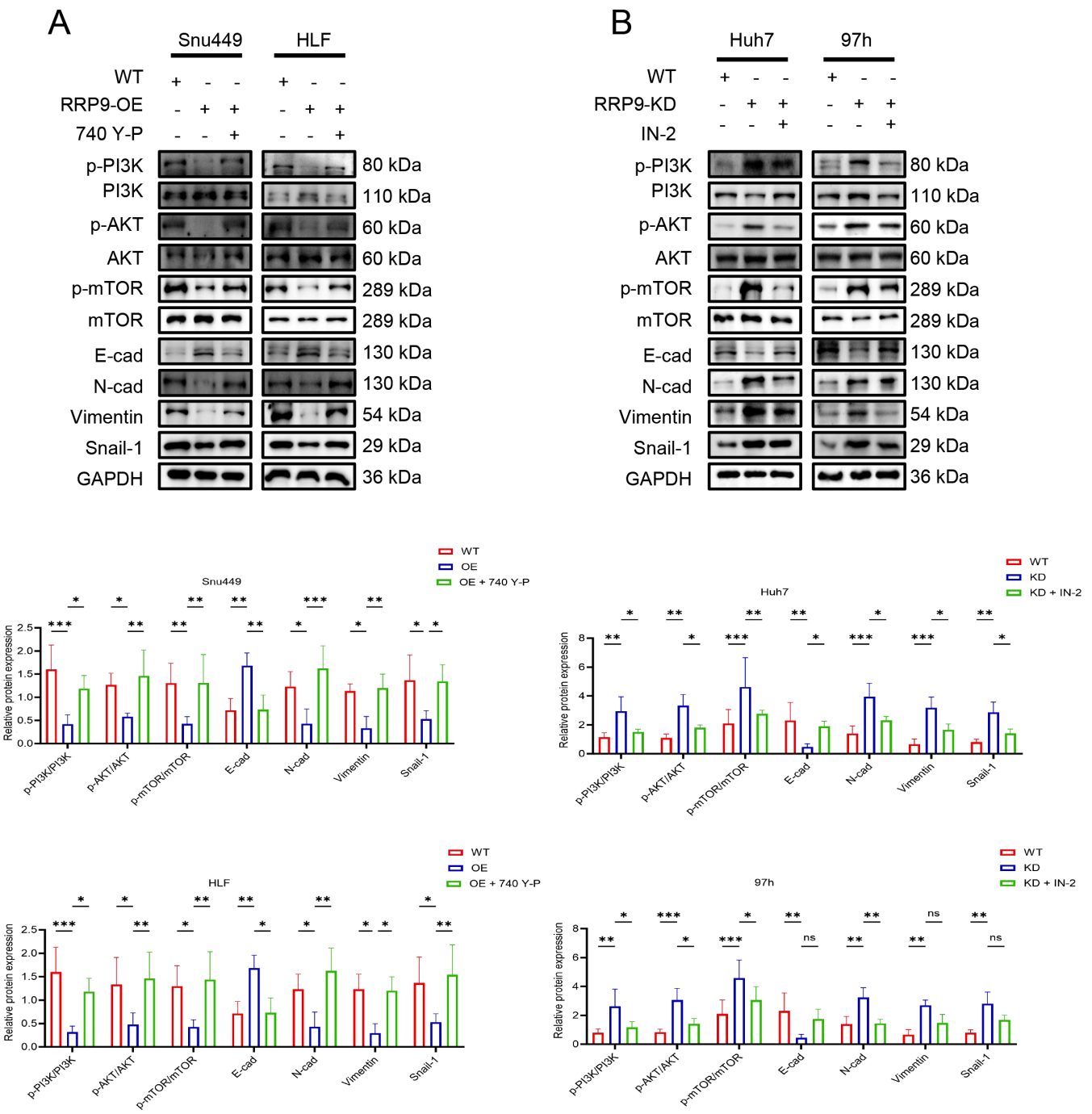

Figure 7. Rescue experiments in cells with RRP9 OE or KD with PI3K/AKT/mTOR pathway activator and inhibitor treatment. (A) Western blot analysis of PI3K, AKT, mTOR, p-PI3K, p-AKT, p-mTOR, E-cad, N-cad, vimentin and Snail-1 protein expression in Snu449 and HLF cells following RRP9 overexpression and (B) Huh7 and 97h cells following RRP9 knockdown. *P<0.05, **P<0.01, ***P<0.001. RRP9, ribosomal RNA processing 9; OE, overexpression; KD, knockdown; p-, phosphorylated-; E-cad, epithelial cadherin; N-cad, neural cadherin; WT, wild-type; IN-2, PI3K/Akt/mTOR-IN-2.

lose apical-basal polarity and tight intercellular junctions, acquiring mesenchymal characteristics (34). This conversion enhances cell migratory and invasive ability, confers resistance to therapeutic agents and allows evasion of immune surveillance (34). Apoptosis, a highly regulated form of programmed cell death, serves a key tumor-suppressive role (35). EMT and apoptosis are key for cancer promotion and suppression, respectively, making it crucial to understand the association between RRP9 and these processes in HCC. snoRNAs are involved in the post-transcriptional modification and maturation of rRNA, which is key for ribosome biogenesis. Increasing evidence has implicated dysregulated snoRNAs in the development of multiple types of cancer, including HCC, colorectal cancer and pancreatic ductal adenocarcinoma (18,36,37). snoRNAs are classified into seven families, U1-U7, based on their high U content (20,38). The present study demonstrated that RRP9/U3-55K, a core subunit of the U3-snoRNP complex (19), exerts tumor-suppressive activity in HCC. This is in contrast with its established oncogenic roles in pancreatic, breast, and colorectal cancer, where it drives malignant progression by constitutively activating AKT signaling, promoting chemoresistance and interacting with proteins such

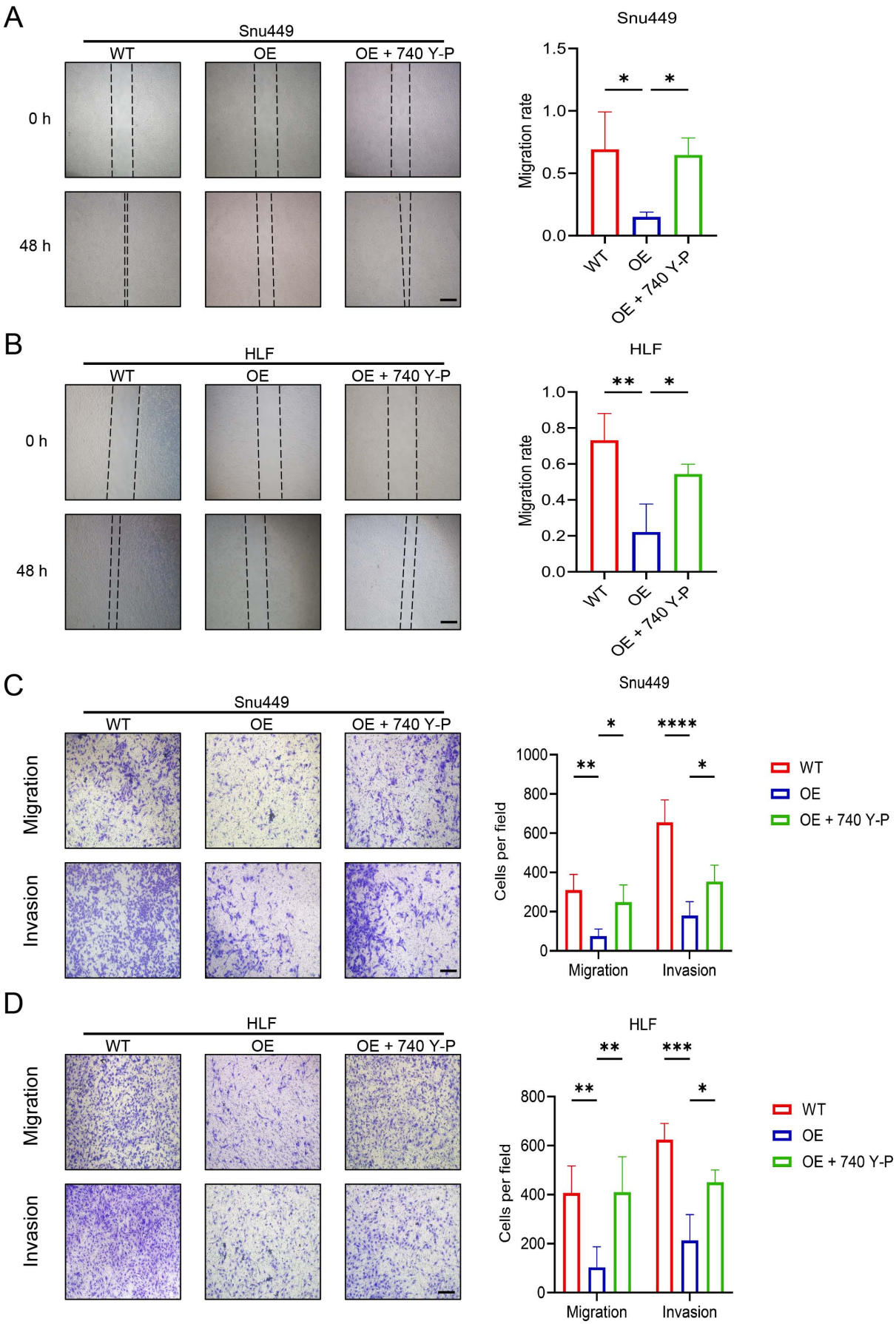

Figure 8. Rescue experiments using 740 Y-P in RRP9-OE Snu449 and HLF cells. (A) Wound healing assay evaluating the migration of Snu449 and (B) Wound healing assay evaluating the migration of HLF cells. (C) Transwell assays assessing the migration and invasion of Snu449 cells in the WT, OE, and OE + 740 Y-P groups. (D) Transwell assays assessing the migration and invasion of HLF cells in the WT, OE, and OE + 740 Y-P groups. Scale bar, 100 μm. *P<0.05, **P<0.01, ***P<0.001, ****P<0.0001. RRP9, ribosomal RNA processing 9; OE, overexpression; WT, wild-type.

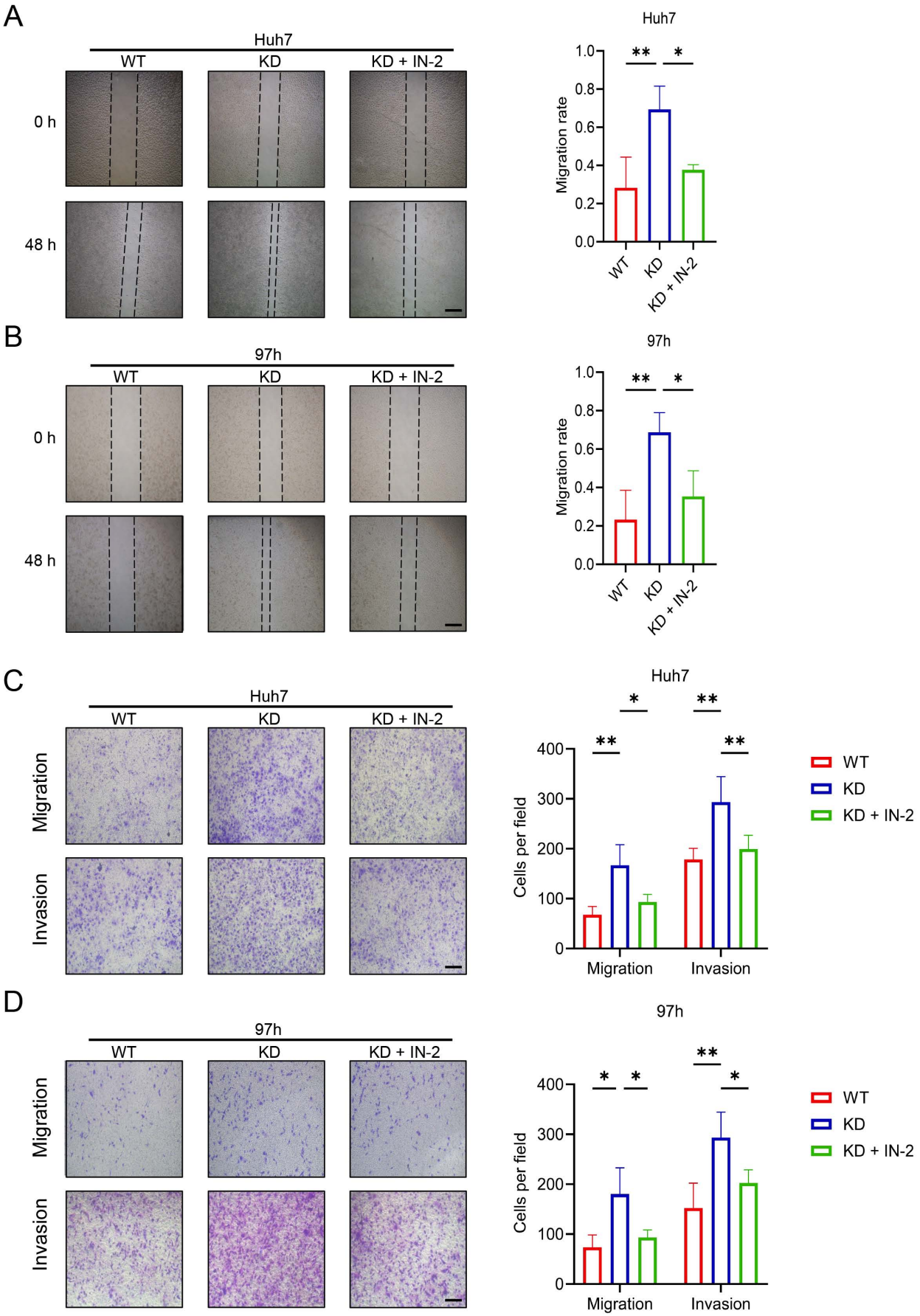

Figure 9. Rescue experiments using ribosomal RNA processing 9 KD 97h and Huh7 cells treated with PI3K/AKT/mTOR pathway inhibitor. (A) Wound healing assay evaluating the migration of Huh7 and (B) 97h cells in the WT, KD, and KD + IN-2 groups. (C) Transwell assays assessing the migration and invasion of Huh7 cells in the WT, KD, and KD + IN-2 groups. (D) Transwell assay of migration and invasion of 97h cells in the WT, KD, and KD + IN-2 groups. Scale bar, 100 μm. *P<0.05, **P<0.01. KD, knockdown; IN-2, PI3K/Akt/mTOR-IN-2; WT, wild-type.

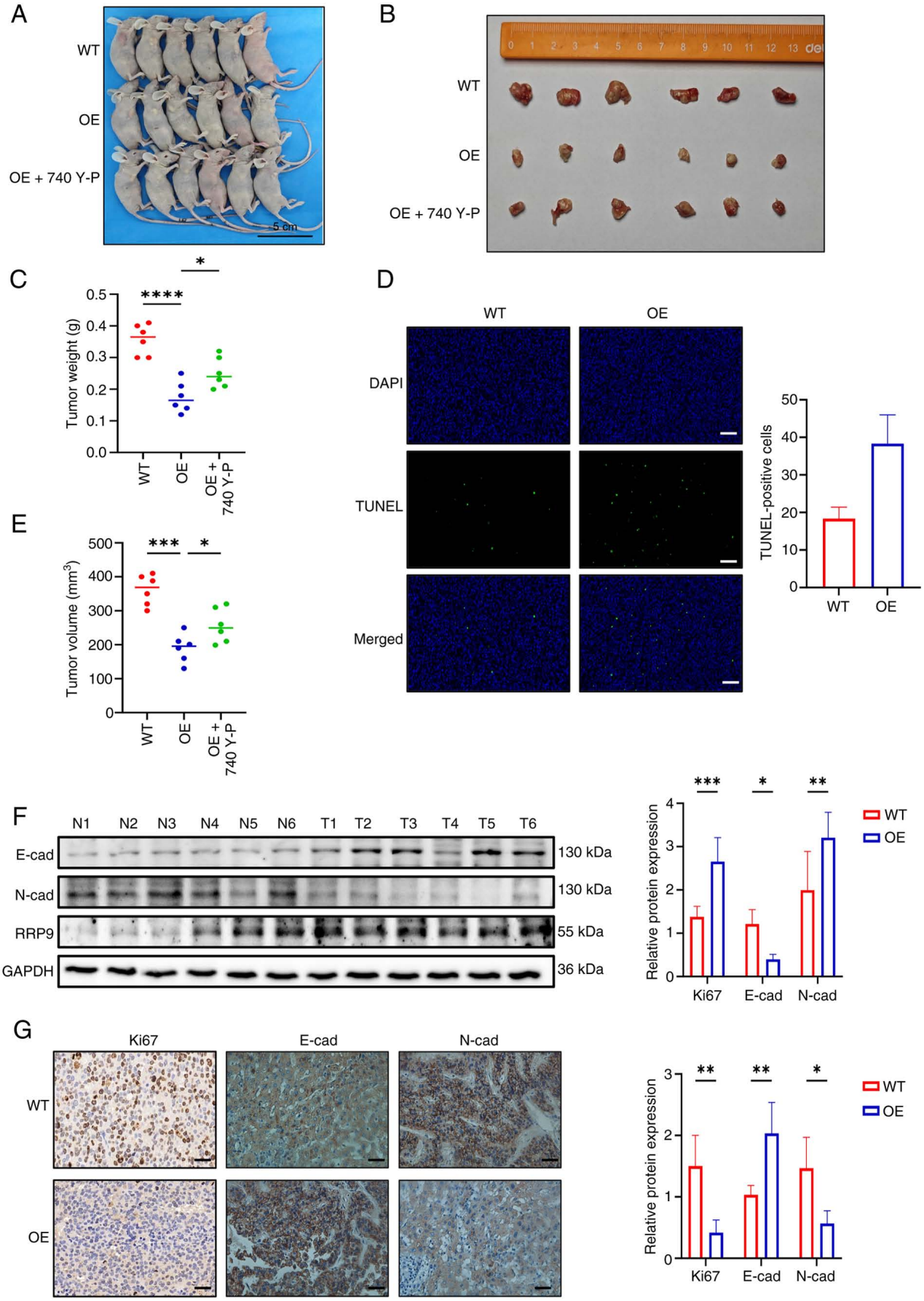

Figure 10. *In vivo* validation of RRP9 role in tumor progression. (A) Mice on day 14 post-injection. (B) Xenograft tumors excised from nude mice. Xenograft (C) tumor weight and (D) volume. (E) TUNEL staining. (F) Western blot analysis of RRP9, E-cad and N-cad protein expression in WT and OE groups. (G) Immunohistochemistry analysis of Ki67, E-cad and N-cad expression in xenograft tumor tissues. Scale bar, 100 μm. *P<0.05, **P<0.01, ***P<0.001 ****P<0.0001. RRP9, ribosomal RNA processing 9; E-cad, epithelial cadherin; N-cad, neural cadherin; WT, wild-type; OE, overexpression.

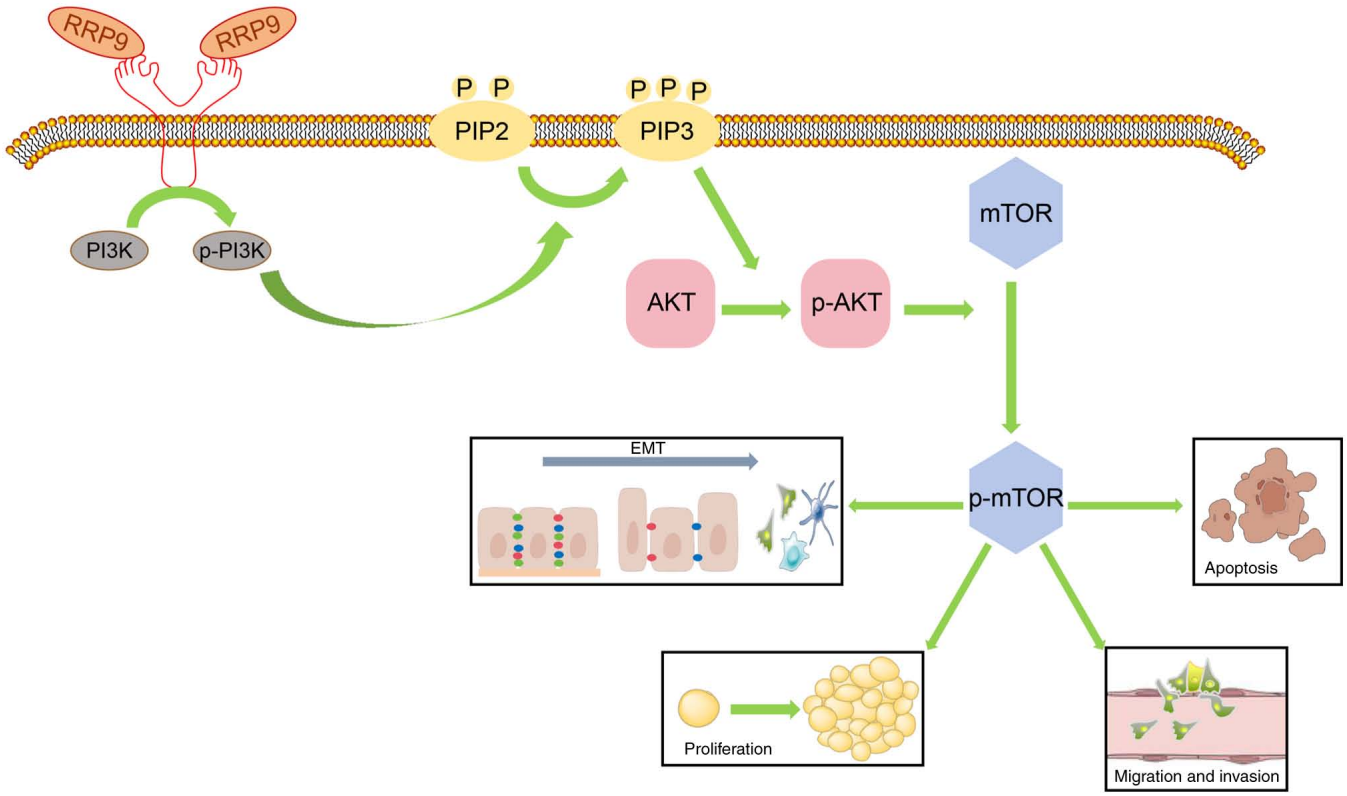

Figure 11. RRP9 regulates the PI3K/AKT/mTOR signaling pathway. RRP9, ribosomal RNA processing 9; p-, phosphorylated-; PIP2, phosphatidylinositol 4,5-bisphosphate; EMT, epithelial-mesenchymal transition.

as JUN and DExD-box helicase 21 (22,23,39,40). RRP9 interacts with distinct signaling molecules or proteins in different cancer contexts, yielding opposing regulatory outcomes; this highlights the context-dependent nature of RRP9 functionality and provides a direction for future research.

To elucidate the mechanism of action of RRP9 in HCC, HCC cell lines were constructed with either RRP9 overexpression or knockdown. RRP9 significantly inhibited tumor cell proliferation, invasion and migration, while simultaneously promoting apoptosis and suppressing EMT, thereby exerting a notable tumor-suppressive effect. The PI3K/AKT/mTOR signaling pathway is key for HCC metabolism and malignant biological behavior such as proliferation, invasion and migration (41). PI3K activation catalyzes the conversion of phosphatidylinositol diphosphate to phosphatidylinositol triphosphate on the cell membrane, which activates AKT. Activated AKT triggers biological effects by phosphorylating downstream substrates, including mTOR and glycogen synthase kinase-3β (42) (Fig. 11). Inactivation of this pathway inhibits HCC development (43,44). RRP9 modulates the invasion, migration and EMT of HCC cells via the PI3K/AKT/mTOR signaling pathway. Furthermore, RRP9 was shown to impact HCC progression by inhibiting this pathway *in vivo*. Although previous studies have suggested that RRP9 activates the PI3K/AKT/mTOR pathway (22,23), the present study observed the opposite effect. To explore the association between RRP9 and CCNA2, co-IP was performed, which confirmed that RRP9 interacted with CCNA2. Furthermore, the present study demonstrated that CCNA2 regulated the PI3K/AKT/mTOR pathway, linking RRP9-mediated effects to this signaling cascade.

While the present PPI network and co-IP data suggested an interaction between RRP9 and CCNA2 and western blot analysis confirmed that RRP9 modulates CCNA2 protein levels, the precise nature of this regulation requires further investigation. Future studies should determine whether RRP9 directly regulates CCNA2 at the transcriptional level by influencing its promoter activity or at the post-transcriptional level by affecting mRNA stability. Moreover, the specific mechanism by which CCNA2, a key regulator of the cell cycle, influences the PI3K/AKT/mTOR signaling pathway in HCC warrants further exploration. Future studies should use techniques such as luciferase reporter assays to assess transcriptional regulation and RNA immunoprecipitation to examine potential binding to CCNA2 mRNA to determine whether the effects of RRP9 on the PI3K/AKT/mTOR pathway and HCC progression are functionally dependent on CCNA2. Clarifying the precise upstream-to-downstream regulatory sequence and the functional dependencies within the RRP9/CCNA2/PI3K/AKT/mTOR pathway may provide more comprehensive understanding of tumor suppression in HCC.

Given the contrasting oncogenic roles of RRP9 reported in pancreatic, breast and colorectal cancer, its tumor-suppressive activity in HCC may be shaped by a broader regulatory landscape (22-24). In addition to the CCNA2-mediated regulatory axis, other mechanisms may underlie the context-dependent role of RRP9 in modulating PI3K/AKT/mTOR signaling in HCC. First, post-translational modifications of RRP9 affect its function. For example, RRP9 has been reported to undergo neddylation by the ubiquitin-like modifier Nedd8 via the E3

ligase Smurf1, which enhances its activity in tumorigenesis in colorectal cancer models; this demonstrates that RRP9 function is dynamically regulated by covalent modification and changes in such modifications may alter downstream signaling outcomes (45). Moreover, acetylation and deacetylation of RRP9 modulate its binding to U3 snoRNA and influence ribosome biogenesis, suggesting that additional post-translational modifications such as phosphorylation, methylation or ubiquitination may similarly regulate RRP9 interactions and downstream effects in a cell type-specific manner (46,47). Second, tumor- or tissue-specific cofactors and interacting partners may direct RRP9 toward distinct signaling programs. In pancreatic cancer, for example, RRP9 interacts with insulin-like growth factor 2 mRNA-binding protein 1 to activate AKT signaling and promote chemoresistance, whereas in breast cancer RRP9 interacts with JUN to regulate AKT pathway activity and tumor progression (23). These interactions demonstrate how RRP9 engages different RNA-binding proteins or transcriptional regulators depending on the cell context, thereby altering the downstream impact on PI3K/AKT/mTOR and associated pathways (22,23).

Additionally, differences in upstream regulatory signaling environments across cancer types may shape how RRP9 influences PI3K/AKT/mTOR signaling. The repertoire of activated receptor tyrosine kinases, metabolic state or viral infection status (hepatitis B or C in HCC) may change the balance of interacting signaling nodes available to RRP9 compared with cancer types lacking these stimuli (48,49). Given that snoRNAs and their associated proteins are influenced by broader epigenetic and transcriptional networks in cancer, including other non-coding RNAs that regulate PI3K/AKT activity, these upstream differences may contribute to divergent functional outcomes (50,51).

To the best of our knowledge, the present study is the first to report the tumor-suppressive effect of RRP9, which contrasts with previous findings (23,52). Additionally, the present study demonstrated that RRP9 exerted a tumor-suppressive effect by inhibiting the PI3K/AKT/mTOR pathway. The present study provided key insights into the role of RRP9 in HCC progression and highlights its potential as a therapeutic target.

Acknowledgements

Not applicable.

Funding

The present study was supported by Discipline Construction Funds of Hubei Province (grant no. CZ2025020003-5), Chen Xiao-ping Foundation for the Development of Science and Technology of Hubei Province (grant no. CXPJJH123003-094) and Natural Science Foundation of Hubei Province (grant no. 2023AFB197).

Availability of data and materials

The data generated in the present study may be found in the National Center for Biotechnology Information under accession number PRJNA1330788 or at the following URL: ncbi.nlm.nih.gov.

Authors' contributions

ZF, WW, JF, KD and ML conceived and designed the study. ZF, ML and WW confirm the authenticity of all the raw data. WW and JF provided administrative support. All authors wrote the manuscript. All authors have read and approved the final manuscript.

Ethics approval and consent to participate

The human sample experiments were approved by the Ethics Committee of Wuhan University People's Hospital (Wuhan, China; approval no. WDRY2022-K013) and written informed consent was obtained from all patients prior to participation. The animal experiments were approved by the Animal Research Ethics Committee of Wuhan University People's Hospital (approval no. WDRM20250303).

Patient consent for publication

Not applicable.

Competing interests

The authors declare that they have no competing interests.

References

1. Sung H, Ferlay J, Siegel RL, Laversanne M, Soerjomataram I, Jemal A and Bray F: Global cancer statistics 2020: GLOBOCAN estimates of incidence and mortality worldwide for 36 cancers in 185 countries. CA Cancer J Clin 71: 209-249, 2021.
2. Rumgay H, Arnold M, Ferlay J, Lesi O, Cabasag CJ, Vignat J, Laversanne M, McGlynn KA and Soerjomataram I: Global burden of primary liver cancer in 2020 and predictions to 2040. J Hepatol 77: 1598-606, 2022.
3. Hwang SY, Danpanichkul P, Agopian V, Mehta N, Parikh ND, Abou-Alfa GK, Singal AG and Yang JD: Hepatocellular carcinoma: Updates on epidemiology, surveillance, diagnosis and treatment. Clin Mol Hepatol 31 (Suppl): S228-S254, 2025.
4. Toh MR, Wong EYT, Wong SH, Ng AWT, Loo LH, Chow PK and Ngeow J: Global epidemiology and genetics of hepatocellular carcinoma. Gastroenterology 164: 766-782, 2023.
5. Anwanwan D, Singh SK, Singh S, Saikam V and Singh R: Challenges in liver cancer and possible treatment approaches. Biochim Biophys Acta Rev Cancer 1873: 188314, 2020.
6. Galicia-Moreno M, Silva-Gomez JA, Lucano-Landeros S, Santos A, Monroy-Ramirez HC and Armendariz-Borunda J: Liver cancer: Therapeutic challenges and the importance of experimental models. Can J Gastroenterol Hepatol 2021: 8837811, 2021.
7. Liang J, Wen J, Huang Z, Chen XP, Zhang BX and Chu L: Small nucleolar RNAs: Insight into their function in cancer. Front Oncol 9: 587, 2019.
8. Pecoraro A, Pagano M, Russo G and Russo A: Ribosome biogenesis and cancer: Overview on ribosomal proteins. Int J Mol Sci 22: 5496, 2021.
9. Gaviraghi M, Vivori C and Tonon G: How cancer exploits ribosomal RNA biogenesis: A journey beyond the boundaries of rRNA transcription. Cells 8: 1098, 2019.
10. Elhamamsy AR, Metge BJ, Alsheikh HA, Shevde LA and Samant RS: Ribosome biogenesis: A central player in cancer metastasis and therapeutic resistance. Cancer Res 82: 2344-2353, 2022.
11. Lorenzo HK: Small nucleolar RNAs as emerging players in cancer biology and precision medicine. Cancers (Basel) 17: 3847, 2025.
12. Gee HE, Buffa FM, Camps C, Ramachandran A, Leek R, Taylor M, Patil M, Sheldon H, Betts G, Homer J, *et al*: The small-nucleolar RNAs commonly used for microRNA normalisation correlate with tumour pathology and prognosis. Br J Cancer 104: 1168-1177, 2011.

13. Blenkiron C, Hurley DG, Fitzgerald S, Print CG and Lasham A: Links between the oncoprotein YB-1 and small non-coding RNAs in breast cancer. PLoS One 8: e80171, 2013.
14. Yang X, Li Y, Li L, Liu J, Wu M and Ye M: SnoRNAs are involved in the progression of ulcerative colitis and colorectal cancer. Dig Liver Dis 49: 545-551, 2017.
15. Yoshida K, Toden S, Weng W, Shigeyasu K, Miyoshi J, Turner J, Nagasaka T, Ma Y, Takayama T, Fujiwara T and Goel A: SNORA21-an oncogenic small nucleolar RNA, with a prognostic biomarker potential in human colorectal cancer. EBioMedicine 22: 68-77, 2017.
16. Wu L, Zheng J, Chen P, Liu Q and Yuan Y: Small nucleolar RNA ACA11 promotes proliferation, migration and invasion in hepatocellular carcinoma by targeting the PI3K/AKT signaling pathway. Biomed Pharmacother 90: 705-712, 2017.
17. Li G, He Y, Liu X, Zheng Z, Zhang M, Qin F and Lan X: Small nucleolar RNA 47 promotes tumorigenesis by regulating EMT markers in hepatocellular carcinoma. Minerva Med 108: 396-404, 2017.
18. Cui L, Nakano K, Obchoei S, Setoguchi K, Matsumoto M, Yamamoto T, Obika S, Shimada K and Hiraoka N: Small nucleolar noncoding RNA SNORA23, up-regulated in human pancreatic ductal adenocarcinoma, regulates expression of spectrin repeat-containing nuclear envelope 2 to promote growth and metastasis of xenograft tumors in mice. Gastroenterology 153: 292-306.e2, 2017.
19. Clerget G, Bourguignon-Igel V, Marmier-Gourrier N, Rolland N, Wacheul L, Manival X, Charron C, Kufel J, Méreau A, Senty-Ségault V, *et al*: Synergistic defects in pre-rRNA processing from mutations in the U3-specific protein Rrp9 and U3 snoRNA. Nucleic Acids Res 48: 3848-3868, 2020. DOI: 10.1093/nar/gkaa066.
20. Ojha S, Malla S and Lyons SM: snoRNPs: Functions in ribosome biogenesis. Biomolecules 10: 783, 2020.
21. Beltrame M and Tollervey D: Base pairing between U3 and the pre-ribosomal RNA is required for 18S rRNA synthesis. EMBO J 14: 4350-4356, 1995.
22. Zhang Z, Yu H, Yao W, Zhu N, Miao R, Liu Z, Song X, Xue C, Cai C, Cheng M, *et al*: RRP9 promotes gemcitabine resistance in pancreatic cancer via activating AKT signaling pathway. Cell Commun Signal 20: 188, 2022.
23. Huan J, Liu X, Wang N, Mu Y, Li L and Du Y: The RRP9-JUN axis promotes breast cancer progression via the AKT signalling pathway. Biol Direct 19: 131, 2024.
24. Liu H, Chi X, Yang N, Shan M, Xiao Y, Zhang M, Hao Y, Hou S, Liu Y and Wang Y: Joint effect of RRP9 and DDX21 on development of colorectal cancer and keloid. Aging (Albany NY) 15: 14703-14719, 2023.
25. Qin J, Sun X, Ma Y, Cheng Y, Ma Q, Jing W, Qu S and Liu L: Design, synthesis and biological evaluation of novel 1,3,4,9-tetrahydropyrano[3,4-b]indoles as potential treatment of triple negative breast cancer by suppressing PI3K/AKT/mTOR pathway. Bioorg Med Chem 55: 116594, 2022.
26. An Y, Cao C, Sun S, Wu H, Zhang J, Li R and Zhao Y: SHP1 and its downstream p38/SP1/PI3K/YAP/Notch-1 signaling in trophoblast cells suppressed the progression of Preeclampsia via inhibiting proliferation of SMCs. Sci Rep 15: 16205, 2025.
27. Amin MB, Greene FL, Edge SB, Compton CC, Gershenwald JE, Brookland RK, Meyer L, Gress DM, Byrd DR and Winchester DP: The eighth edition AJCC cancer staging manual: Continuing to build a bridge from a population-based to a more 'personalized' approach to cancer staging. CA Cancer J Clin 67: 93-99, 2017.
28. Reig M, Forner A, Rimola J, Ferrer-Fàbrega J, Burrel M, Garcia-Criado Á, Kelley RK, Galle PR, Mazzaferro V, Salem R, *et al*: BCLC strategy for prognosis prediction and treatment recommendation: The 2022 update. J Hepatol 76: 681-693, 2022.
29. Liu T, Shi Q, Yang L, Wang S, Song H, Wang Z, Xu X, Liu H, Zheng H and Shen Z: Long non-coding RNAs HERH-1 and HERH-4 facilitate cyclin A2 expression and accelerate cell cycle progression in advanced hepatocellular carcinoma. BMC Cancer 21: 957, 2021.
30. Gan Y, Li Y, Li T, Shu G and Yin G: CCNA2 acts as a novel biomarker in regulating the growth and apoptosis of colorectal cancer. Cancer Manag Res 10: 5113-5124, 2018.
31. Suski JM, Braun M, Strmiska V and Sicinski P: Targeting cell-cycle machinery in cancer. Cancer Cell 39: 759-778, 2021.
32. Llovet JM, Kelley RK, Villanueva A, Singal AG, Pikarsky E, Roayaie S, Lencioni R, Koike K, Zucman-Rossi J and Finn RS: Hepatocellular carcinoma. Nat Rev Dis Primers 7: 6, 2021.
33. Bray F, Laversanne M, Sung H, Ferlay J, Siegel RL, Soerjomataram I and Jemal A: Global cancer statistics 2022: GLOBOCAN estimates of incidence and mortality worldwide for 36 cancers in 185 countries. CA Cancer J Clin 74: 229-263, 2024.
34. Zhang J, Hu Z, Horta CA and Yang J: Regulation of epithelial-mesenchymal transition by tumor microenvironmental signals and its implication in cancer therapeutics. Semin Cancer Biol 88: 46-66, 2023.
35. Morana O, Wood W and Gregory CD: The apoptosis paradox in cancer. Int J Mol Sci 23: 1328, 2022.
36. Ding Y, Sun Z, Zhang S, Zhou L, Xu Q, Zhou D, Li Y, Han X, Xu H, Bai Y, *et al*: Identification of snoRNA SNORA71A as a novel biomarker in prognosis of hepatocellular carcinoma. Dis Markers 2020: 8879944, 2020.
37. Zhang Z, Tao Y, Hua Q, Cai J, Ye X and Li H: SNORA71A promotes colorectal cancer cell proliferation, migration, and invasion. Biomed Res Int 2020: 8284576, 2020.
38. Dragon F, Gallagher JE, Compagnone-Post PA, Mitchell BM, Porwancher KA, Wehner KA, Wormsley S, Settlage RE, Shabanowitz J, Osheim Y, *et al*: A large nucleolar U3 ribonucleoprotein required for 18S ribosomal RNA biogenesis. Nature 417: 967-970, 2002.
39. Chi X, Yang N and Liu Y: RRP9 and DDX21 as new biomarkers of colorectal cancer. Medicine (Baltimore) 102: e34384, 2023.
40. Li N, Jing Y, Xu L and Wang M: METTL1 enhances RRP9 mRNA stability through m7G modification to drive colorectal tumorigenesis. Mol Carcinog 64: 858-869, 2025.
41. Alzahrani AS: PI3K/Akt/mTOR inhibitors in cancer: At the bench and bedside. Semin Cancer Biol 59: 125-132, 2019.
42. Li Y, Liu Z, Yan H, Zhou T, Zheng L, Wen F, Guo G and Zhang Z: Polygonatum sibiricum polysaccharide ameliorates skeletal muscle aging and mitochondrial dysfunction via PI3K/Akt/mTOR signaling pathway. Phytomedicine 136: 156316, 2025.
43. Chen J, Chen J, Huang J, Li Z, Gong Y, Zou B, Liu X, Ding L, Li P, Zhu Z, *et al*: HIF-2α upregulation mediated by hypoxia promotes NAFLD-HCC progression by activating lipid synthesis via the PI3K-AKT-mTOR pathway. Aging (Albany NY) 11: 10839-10860, 2019.
44. Yang J, Pi C and Wang G: Inhibition of PI3K/Akt/mTOR pathway by apigenin induces apoptosis and autophagy in hepatocellular carcinoma cells. Biomed Pharmacother 103: 699-707, 2018.
45. Du MG, Liu F, Chang Y, Tong S, Liu W, Chen YJ and Xie P: Neddylation modification of the U3 snoRNA-binding protein RRP9 by Smurf1 promotes tumorigenesis. J Biol Chem 297: 101307, 2021.
46. Chen S, Blank MF, Iyer A, Huang B, Wang L, Grummt I and Voit R: SIRT7-dependent deacetylation of the U3-55k protein controls pre-rRNA processing. Nat Commun 7: 10734, 2016.
47. Modenini G, Abondio P and Boattini A: The coevolution between APOBEC3 and retrotransposons in primates. Mob DNA 13: 27, 2022.
48. Chen X, Wang X, Zhu F, Qian C, Xu F, Huang X, Zhang W and Sun B: HBV infection-related PDZK1 plays an oncogenic role by regulating the PI3K-Akt pathway and fatty acid metabolism and enhances immunosuppression. J Immunol Res 2022: 8785567, 2022.
49. Qu H, Xie Y, Hu S, Sun S, Yuan Y, Xia Y, Liu M and Zhang XL: HBV upregulates TNNT1 expression through PI3K/AKT/mTOR-c-Myc axis, which in turn induces EMT and liver fibrosis in mice. Cell Signal 134: 111899, 2025.
50. Hussain MS, Moglad E, Afzal M, Gupta G, Hassan Almalki W, Kazmi I, Alzarea SI, Kukreti N, Gupta S, Kumar D, *et al*: Non-coding RNA mediated regulation of PI3K/Akt pathway in hepatocellular carcinoma: Therapeutic perspectives. Pathol Res Pract 258: 155303, 2024.
51. Zacchini F, Barozzi C, Venturi G and Montanaro L: How snoRNAs can contribute to cancer at multiple levels. NAR Cancer 6: zcae005, 2024.
52. Wang Z, Zhao C, Li M, Zhang L, Diao J, Wu Y, Yang T, Shi M, Lei Y, Wang Y, *et al*: Tuina therapy alleviates knee osteoarthritis by modulating PI3K/AKT/mTOR-mediated autophagy: An integrated machine learning and in vivo rat study. Front Immunol 16: 1635818, 2025.